Effect of Various Phase Fractions of Bainite, Retained Austenite, Intercritical Ferrite and Pearlite on the Crevice Corrosion Behaviour of Multiphase steels

Neetu, S. Sangal and K. Mondal
Department of Materials Science and Engineering,
Indian Institute of Technology Kanpur, Kanpur 208016, India

Abstract: Crevice corrosion occurs between the rail components, such as rail clip and insert, rail clip and liner, rail foot and liner, etc. Since the crevice corrosion of these rail components is of major concern as metal dissolution can cause the loosening of the assembly and lack of performance, the present work concentrates on finding the crevice corrosion behaviour of the developed multiphase bainitic EN 45 grade steels. The severity of crevice corrosion has been investigated by studying the surface dissolution and the rust formed on the exposed surfaces of the steels after the crevice test in 3.5 wt.% NaCl solution. SEM and optical profilometry have been used for the analysis of surface dissolution behaviour. Moreover, the rust formed on the exposed surfaces has been characterized using SEM, and it shows the presence of various rust phases, such as α FeOOH, β FeOOH, γ FeOOH, α Fe_2O_3, etc. Furthermore, Raman spectroscopy has been used for the confirmation and quantification of these rust phases. The higher protective ability index (PAI) calculated from the Raman spectroscopy shows the higher corrosion resistance of the multiphase bainitic steels. Here, multiphase interaction and rust constituents uniquely control the corrosion of the developed bainitic steels.

Keywords: Multiphase steel (MPS); Crevice corrosion; Raman spectroscopy; Optical profilometry.

1. Introduction

In order to meet the demands of heavy traffic conditions and the need for the movement of huge amounts of weight, now a days, various researches are now focused on improving the strength along with toughness of railroad comproments.[1–10] Corrosion behaviour of these railroad components is also a crucial parameter in addition to strength. For the locomotives to operate properly, various railroad components such as wheel axle, rail clip, etc. are interconnected. However, a small gap between these connected components can form crevices and affect their corrosion behaviour due to entrapment of the acidic solution. Hence, there is a need to improve crevice corrosion resistance of these railroad components which can be done either by alteration of alloying elements or by morphological changes.

Bainitic steels can be a promising candidate for the railway application due to their high mechanical strength as well as the high toughness and ductility.[1–4,11] Moon et al.[1-] have reported that the conventional C Mn rail steel shows ~880 MPa tensile strength with 12% elongation while the bainitic steel (0.71C 0.35Si 1.15Mn) (wt.%) shows ~1300 MPa tensile strength with 10% elongation. Moon et al.[12] have further studied the axle steels and reported ~600 MPa tensile strength with 25% elongation of conventional axle steel and ~1100 MPa tensile strength with 15% elongation of the newly developed bainitic steel (0.19C 0.34Si 1.32Mn) (wt.%) for axles. Furthermore, Katiyar et al.[12] have studied the mechanical behaviour of high C rail steel (0.70C 0.24Si 1.12Mn) (wt.%) with the microstructural variation developed via different heat treatment routes and reported that the bainitic rail steel shows higher hardness compared to pearlitic, tempered martensitic and spheroidized steels.[2] Proper alloying and combinations of austempering temperature and holding duration could develop a bainitic steel with extraordinary strength and ductility. Aglan et al.[1] have reported ~1500 MPa tensile strength with ~13% elongation of the bainitic rail steel (0.23C 1.96Si) (wt.%).[1] Moreover, Amel Farzad et al.[9]

have reported ~ 700 HV hardness of a bainitic steel containing few nanometres of bainitic ferrite lath thickness.[9] They have developed nanostructured bainite at austempering range of 200^{0}C to 300^{0}C using 1.15C 2.15Si 1.58Co (wt.%) steel.

Combinations of austempering temperatures and holding durations could produce other phases along with the bainite. These dual phase or multiphase steels possess excellent mechanical properties.[1–9] Bakhtiari et al.[4] have developed dual phase bainitic 34%ferritic steel (0.44C 0.29Si 0.72Mn) (wt.%) with lower and upper bainitic structures at austempering range of 300^{0}C-450^{0}C[4]. They have reported that the lower bainitic ferritic steel developed at 300^{0}C exhibits ~1400 MPa tensile strength with ~21% elongation while upper bainitic ferritic steel developed at 450^{0}C exhibits ~1500 MPa tensile strength with ~17% elongation.

Furthermore, bainitic steels offer good corrosion resistance along with the strong mechanical strength.[12, 20] Kazum et al. have reported that the 0.79C 1.5Si 1.98Mn 0.98Cr (wt.%) steel with nanostructured bainite shows a higher corrosion resistance than with the martensite structure in 3.5% NaCl solution.[18] They have observed that the martensitic steel shows high localized corrosion where grain boundaries predominantly lead to intergranular corrosion while the bainitic steel exhibits general uniform corrosion resulting in the lower dissolution. Wang et al. have used 0.023C 0.3Si 1.63Mn (wt.%) ultra low carbon steel and developed bainitic structure via austempering at 650^{0}C with 60 min of holding.[19] The ultra low carbon bainitic steel shows increased corrosion resistance than the 09CuPCrNi weathering steel due to the low carbon content, homogenous microstructure and presence of high amount of low angle grain boundaries. Barraza Fierro et al. have applied different thermomechanical treatments on two different compositions of steel to develop 98% bainite martensite and 32%[7] bainite martensite. They have reported higher mechanical strength as well as the charge transfer resistance (corrosion resistance) of the 98% bainite martensite steel.

Due to high strength and adequate ductility, steels with a high C and high Si content are typically used for railroad components. Varshney et al.[21] have developed a series of multiphase bainitic steels with base composition, 0.61C 1.71Si 0.86Mn (wt.%), with some other phases/microconstituents such as retained austenite (RA), intercritical ferrite (IF) and pearlite using various combinations of continuous cooling durations before isothermal holding and austempering temperatures and reported maximum of ~2 GPa tensile strength with ~10% elongation. Furthermore, Neetu et al. have studied the immersion and electrochemical corrosion behaviour of the same moderately high C high Si multiphase bainitic steel (developed by a similar method as done by Varshney et al. in 3.5 wt.% NaCl solution and observed that multiphase bainitic steels also exhibit excellent corrosion resistance in the case of both immersion and electrochemical tests.[23] Moreover, Neetu et al. have studied the sliding wear behaviour of the same moderately high C high Si multiphase bainitic steels using pin/ball on disc wear testing machine and observed extraordinary wear resistance due to the presence of various phases.[24] Mechanical strength, corrosion and wear resistance are exclusively controlled by various phases present in the high C high Si multiphase bainitic steels. The comparative study of mechanical properties, corrosion rates and wear volume loss of the multiphase bainitic steel with the conventional rail components (studied by Neetu et al.[23,24]) shows that this steel could be a promising candidate for railway applications.

Service life of the railway components are also affected by the crevice corrosion due to the formation of small gap between the interconnected components. Even though several studies have been performed on the corrosion behaviour of the bainitic steel, it could be highly interesting to evaluate the crevice corrosion behaviour of the high C high Si multiphase steel as it contains excellent mechanical strength, corrosion and wear resistance. Since single composition is used to make the multiphase steels, it could be another reason for the evaluation of crevice corrosion in the present work. Further, lack of the research of the crevice corrosion behaviour of the moderately high C and high Si bainitic steel brings focus on the present work. In light of this, the current study examines the crevice corrosion behaviour of the multiphase steel with a moderately high C (0.67) high Si (1.71) (wt.%) content and the effect of various phases present and their fractions on the dissolution mechanism using 3.5 wt.% NaCl solution. The

present work also focuses on the effect of salinity and total dissolved solids of the NaCl solution as well as the various formed rust phases on the crevice corrosion of the multiphase steel.

2. Experimental procedures

2.1 Materials preparation

The as received steel contains 0.67% C, 1.71% Si, 0.86% Mn, 0.01 Mo, 0.07% Cr, 0.04% Ni and Fe (balance amount) (wt.%). The specimens with 25 mm x 25 mm x 3 mm dimensions were prepared from the as received steel. All the steel specimens were heat treated at 1040^{0}C for 7 min for complete austenitization. Immediately after the complete austenitization, the steel specimens were continuously cooled for 0 s, 10 s, 20 s and 40 s in the still air followed by sudden quenching to different isothermal temperatures (300^{0}C, 350^{0}C and 400^{0}C) with holding for 10 min into the salt bath furnace containing 20% $NaNO_3$ + 80% KNO_3. These specimens were then immediately quenched in water at room temperature for the formation of multiphases. The TTT curve[25] superimposed with the heat treatment cycle for the development of the MPS specimens is shown in Fig. 1a.

Microstructural examination of the multiphase steel (MPS) specimens was executed with the help of and scanning electron microscopy (Nova Nano SEM 450). All the MPS specimens were ground using SiC papers up to 2500 grit size. Further cloth polishing was done with 3 μm and 1 μm alumina suspension, sequentially, followed by etching with 2% nital solution. For the retained austenite identification and its volume fraction calculation, X ray diffraction (XRD) analysis has been performed on the MPS specimens in a Bruker D8 Focus XRD using Cu target (wavelength = 1.54 Å) with 30º to 120º 2θ angle at 30 mA, 40 kV and scanning rate of 0.5º per min. For XRD analysis, the MPS specimens were prepared till the cloth polishing the similar way used in microstructural examination.

2.2 Crevice test

Crevice test of the MPS specimens was carried out in a 3.5 wt.% NaCl solution at room temperature using a crevice setup as per the ASTM standard.[26] All the MPS specimens with 25 mm x 25 mm x 3 mm were prepared similarly as done for microstructural examination up to cloth polishing followed by ultrasonic cleaning with ethanol. Minimum three samples for each condition were prepared for the crevice test. All the MPS specimens fitted with the crevice setups were immersed in the separate glass beakers which were filled with the 350 ml of 3.5 wt.% NaCl solution for 9 months. After 9 months, all the MPS specimens were carefully taken out from the glass beakers followed by drying at the room temperature.

Firstly, the characterization of the rust present on the exposed surfaces of all the MPS specimens were carried out with the help of SEM microscopy (Nova Nano SEM 450). Rust from all the MPS specimens was removed carefully and subjected to Raman spectroscopy for identification and quantification various phases present. A Princeton instrument, STR Raman spectroscopy with TE PMT detector and Nd:YAG laser at 532 nm was used for the Raman spectra analysis. Further the integrated intensities of the Raman peaks correspond to various phases were used for the calculation of the protective ability index (PAI). The PAI (α/γ^*) which signifies the protectiveness of the rust was calculated using the following equation.[27]

$$\frac{\alpha}{\gamma^*} = \frac{Fraction\ \alpha - FeOOH}{Fraction\ (\gamma - FeOOH\ +\ \beta - FeOOH\ +\ Fe_3O_4)} \quad [1]$$

After collecting the rust, all the MPS specimens were cleaned properly using Clark's solution (ASTM G1–03)[28] for the complete removal of rust from the exposed surfaces. After proper cleaning, again weight of all the MPS specimens was measured and weight loss (ΔW) was calculated after 9 months of crevice test using $(W_0 - W_1)/A$ expression. Here, W_0 is the initial weight of the MPS specimen before the crevice test, W_1 is the final weight of the MPS specimen after the crevice test and proper cleaning using Clark's solution, and A is the area of exposed surface (cm^2).

Furthermore, the corrosion rate of all the MPS specimens was calculated with the help of weight loss using following equation (ASTM G1–03)[28]:

$$\text{Corrosion rate (mm/y)} = 3.154 \times 10^8 \times \frac{\Delta w}{\rho A t} \quad [2]$$

Here, Δw = weight loss in g, ρ = density of steel specimens in g/cm^3, A = area of exposed surfaces in cm^2 and t = exposure time in s.

Later, the surface dissolution of the properly cleaned MPS specimens (using Clark's solution[28]) after the crevice test was analysed using SEM and optical profilometry (Bruker GT–KO). It is worth mentioning that no etching has been done on the MPS specimens for understanding the character of surface dissolution using SEM and optical profilometry.

3. Results and discussion

3.1 Microstructural analysis

As received steel contains fully pearlitic structure as shown in Fig. 1b. Further multiphase steels have been developed as explained in the experimental section. SEM micrographs of all the MPS specimens developed at a combination of austempering temperatures (300^{0}C, 350^{0}C and 400^{0}C) and continuous cooling durations (0 s, 10 s, 20 s and 40 s) are shown in Fig. 2. These SEM micrographs clearly exhibit the bainitic morphology. It can be clearly seen that at 300^{0}C austempering lower bainite is formed while at 400^{0}C austempering upper bainite is formed. Austempering at 350^{0}C develops both types of morphologies (mixed morphology of lower + upper bainite). It can also be seen from Fig. 2 that with the variation of continuous cooling durations beside bainite other phases/micro constituents also form. Blocky RA has been observed near the grain boundary region. From the SEM micrographs (Fig. 2) it can be seen that RA formation takes place in all the continuous cooling durations whereas IF phase starts forming at the grain boundary region as the continuous cooling increases beyond 0 s. Pearlite forms when the continuous cooling increases beyond 20 s (Fig. 2d, h and l).

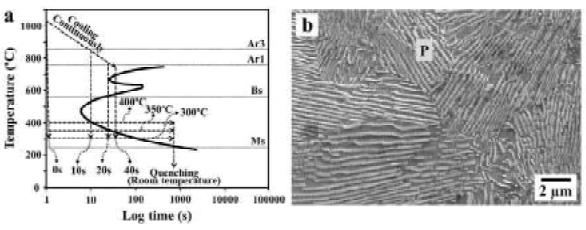


Figure 1. (a) A schematic representation of the TTT curve overlaid with the heat treatment cycles, and (b) SEM micrograph of the as received steel used in the present work for the development of the MPS specimens

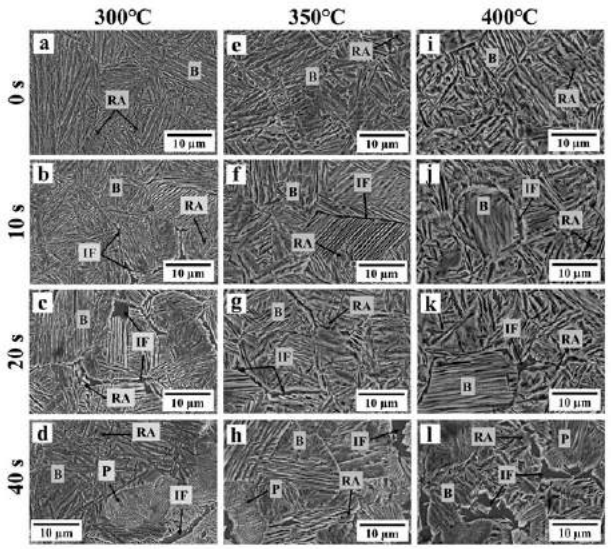


Figure 2. SEM micrograph of the MPS specimens developed at a various combination of austempering temperatures (300^{0}C, 350^{0}C and 400^{0}C) after continuous cooling of 0 s, 10 s, 20 s and 40 s.

Volume fractions of all the phases/micro constituents present in the MPS specimens were calculated using SEM micrographs and XRD analysis and given in Table I. Fig. 3 shows the XRD patterns of all the MPS specimens austempered at various temperatures. XRD patterns clearly show the presence of RA in the MPS specimens. Volume fraction of RA was calculated using a direct comparison method. Remaining bainite, IF and pearlite volume fractions were calculated from the SEM micrographs of the MPS specimens using ImageJ software. For volume fraction analysis, a minimum of ten micrographs were utilized. Here, pixels lying on the various phases/microconstituents, such as pearlite and IF, were counted for the phase fraction analysis using the ImageJ software and these pixel counts were subtracted further from the total counts to get the RA and bainite fractions. Later, the bainite volume fraction was obtained by subtracting the total volume fractions of IF, pearlite and RA (obtained from the XRD analysis) from one. The volume fractions of phases/micro constituents are shown in Table I. These are nearly identical microstructures, as indicated in the work of Varshney et al.,[21,22] since the same heat treatments have been used.

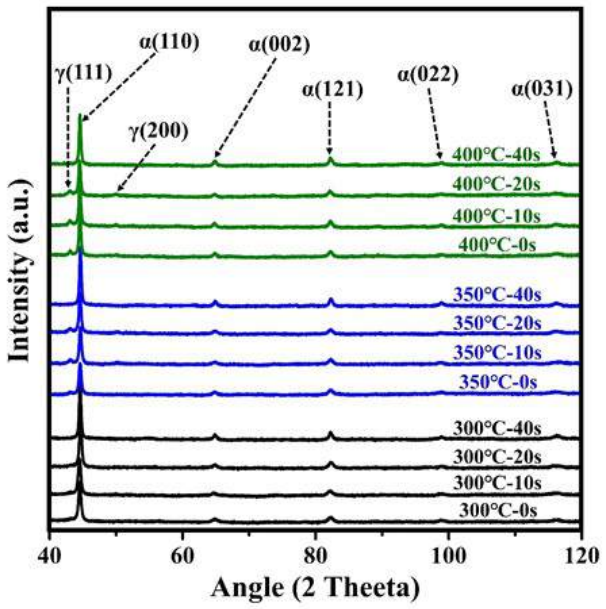


Figure 3. XRD of the MPS specimens developed at a various combination of austempering temperatures (300°C, 350°C and 400°C) after continuous cooling of 0 s, 10 s, 20 s and 40 s.

Bainite volume fraction is observed to be maximum at 0 s of continuous cooling for all three austempering temperature of the MPS specimens and it decreases as the continuous cooling duration increases (Table I). IF volume fraction increases continuously with the increase of continuous cooling durations, whereas RA volume fraction increases till 20 s of continuous cooling and decreases beyond 20 s as pearlite starts forming at 40 s of cooling. MPS specimens austempered at all three temperatures (300°C, 350°C and 400°C) exhibit similar types of volume fractions of phases/micro constituents. At 40 s of continuous cooling, MPS specimens show all 4 types of phases/micro constituents (bainite+ RA+IF+pearlite).

3.2 Crevice test

3.2.1 Weight loss measurement

Fig. 4a and b shows the starting setup for crevice test of the MPS specimens immersed in 3.5 wt.% NaCl solution and after 9 months of crevice test,

Table I. Volume fractions of the phases/micro constituents of the MPS specimens developed at various austempering temperatures (300°C, 350°C and 400°C) after continuous cooling of 0 s, 10 s, 20 s and 40 s.[21,24]

Austempering temperature (°C)	Cooling time (s)	Bainite	Retained Austenite	Intercritical Ferrite	Pearlite
300	0	0.932±0.025	0.068±0.002	0	0
	10	0.878±0.013	0.070±0.003	0.052±0.013	0
	20	0.663±0.028	0.084±0.001	0.253±0.028	0
	40	0.253±0.036	0.058±0.007	0.514±0.038	0.170±0.009
350	0	0.834±0.031	0.166±0.012	0	0
	10	0.736±0.027	0.181±0.004	0.083±0.003	0
	20	0.444±0.038	0.189±0.005	0.367±0.038	0
	40	0.214±0.040	0.071±0.007	0.528±0.026	0.185±0.030
400	0	0.871±0.004	0.123±0.006	0	0
	10	0.775±0.025	0.120±0.007	0.111±0.025	0
	20	0.583±0.039	0.179±0.007	0.237±0.039	0
	40	0.316±0.034	0.008±0.001	0.504±0.045	0.172±0.28

respectively. The average weight loss (g/cm^2) and average corrosion rates (mm/y) of the MPS specimens obtained after 9 months of crevice test in 3.5 wt.% NaCl solution are given in Table II. The average weight loss of the MPS specimens is obtained from three different specimens for each continuous cooling condition at a particular austempering temperature. The weight loss has been calculated after chemical removal of the rusts as indicated in the experimental details. Corrosion rate (mm/y) is calculated with the help of weight loss by using Eq. 2. It has been observed that the corrosion rates of the MPS specimens for all three austempering temperatures gradually increase with the increase in continuous cooling till 20 s followed by a decrease in corrosion rate with 40 s of continuous cooling. The decrease of bainite and increase of RA and IF volume fractions with the increase of continuous cooling duration could increase the corrosion rate of the MPS specimens with the increase of continuous cooling till 20 s. Furthermore, the decrease of RA volume fraction and formation of pearlite with an increase of continuous cooling beyond 20 s decreases the corrosion rate of the MPS specimens. Similar trend of corrosion rate variation after the crevice test of the MPS specimens (Table II) has also been observed after the immersion test of the MPS specimens in 3.5 wt% NaCl solution, the work carried out by the current authors.[23]

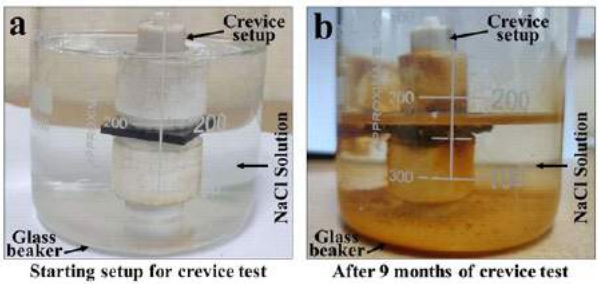


Figure 4. Crevice corrosion setup (a) starting setup for crevice test and (b) after 9 months of crevice test.

Table II. Weight loss, corrosion rate (CR), surface roughness (R_a), Pit depth (R_v) and protective ability index (PAI) values of the MPS specimens after crevice test in 3.5 wt.% NaCl solution.

Austempering temperature (°C)	Cooling time (s)	Weight loss (g/cm^2)	Average Corrosion rate (mm/y)	Average R_a (µm)	Average R_v (µm)	PAI (α/γ^*)
300	0	0.307	0.529	9.3	51.1	0.211
	10	0.365	0.630	9.8	63.9	0.203
	20	0.378	0.652	11.1	70.2	0.182
	40	0.372	0.641	10.3	65.3	0.185
350	0	0.380	0.655	12.1	65.5	0.177
	10	0.405	0.698	12.4	71.2	0.164
	20	0.424	0.732	13.3	73.7	0.151
	40	0.407	0.702	11.9	66.4	0.156
400	0	0.478	0.823	11.6	72.4	0.124
	10	0.521	0.897	13.1	78.6	0.122
	20	0.615	1.059	14.9	110.1	0.109
	40	0.593	1.021	13.9	106.7	0.115

3.2.2 Raman spectroscopy

Fig. 5 shows the Raman spectra of the rusts formed on the exposed surfaces of all the MPS specimens (developed with various combinations of continuous cooling durations and austempering temperatures) after the crevice test in 3.5 wt.% NaCl solution. It can be observed that in spite of variation in austempering temperatures and continuous cooling durations of the MPS specimens, almost similar types of rust phases are formed. Raman spectra show the various peaks related to α FeOOH (goethite), β FeOOH (akaganeite), γ FeOOH (lepidocrocite) and α Fe_2O_3 (haematite). The α FeOOH peaks have been observed at 379 cm^{1}, while the γ FeOOH peaks have been observed at 250 cm^{-1}, 524 cm^{-1} and 1297 cm^{1}.[29] The peaks of α Fe_2O_3 and Fe_3O_4 (magnetite) have also been identified at 219 cm^{1} and 653 cm^{1}, respectively.[30] The peaks of β FeOOH can also be identified at 308 cm^{1}.[29] The possibility of formation of β FeOOH phase has increased since the crevice test is performed in 3.5 wt.% NaCl solution.[31–33] All these rust phases have been observed on the corroded surfaces of all the developed MPS specimens, but their fractions can vary. The presence of different phases/ microconstituents (such as bainite, IF, RA and pearlite) and their different volume fractions in the MPS specimens lead to varying fraction of rust phases (Table II).

Protective ability index (PAI) values have been calculated using α/γ*, as given in Eq. 1, for each MPS specimen (Table II). It has been observed from Table II that the PAI values of the MPS specimens decrease with an increase in continuous cooling till 20 s followed by an increase in PAI value for 40 s of continuous cooling time (Table II). Similar behaviour of the PAI values has been observed for the MPS specimens developed at the other two austempering temperatures (350^{0}C and 400^{0}C). Higher volume fraction of protective α-FeOOH being the most stable rust phase results in higher PAI of the multiphase steel [27]. The MPS specimen developed at 300^{0}C of austempering after 0 s of continuous cooling shows the presence of higher amount of α-FeOOH rust phase resulting in higher PAI compared to the MPS specimens developed using 10 s, 20 s and 40 s continuous cooling [Table II]. It can be clearly seen from Fig. 2 that the MPS specimens developed using

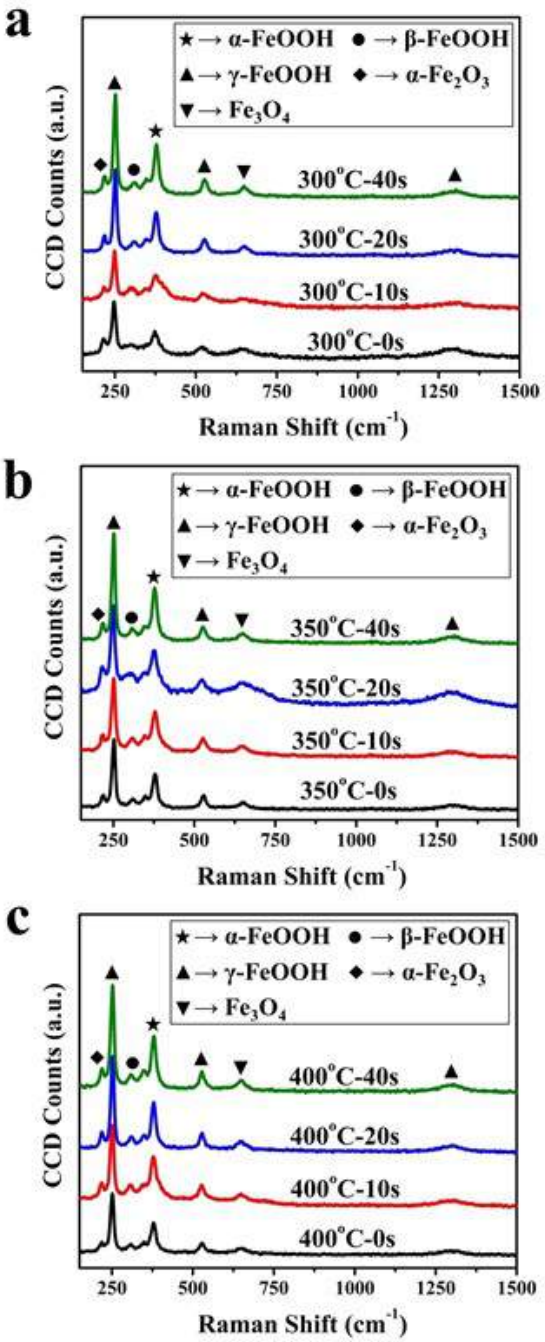


Figure 5. Raman spectra of rust products of the MPS specimens developed at various austempering temperatures (a) 300ºC, (b) 350ºC and (c) 400ºC with the variation of continuous cooling time of 0 s, 10 s, 20 s and 40 s after crevice test in 3.5 wt.% NaCl solution.

0 s of continuous cooling consist of only bainite and some amount of RA. Absence of IF at 0 s of continuous cooling results in lower dissolution as well as higher α-FeOOH fraction. In addition, the PAI values of the MPS specimens austempered at all three temperatures without continuous cooling are found to be highest as compared to the other cooling durations of the respective austempering temperature. Interestingly, the weight loss as well as corresponding corrosion rate data for the MPS specimens after the crevice test show excellent corroboration with the variation of PAI values. The general observation is that the higher the PAI value, the lower is the corrosion rate and weight loss. A similar type of inverse relation of the PAI value with the corrosion rate has also been reported in previous studies.[30,34,35]

3.3.3 Rust morphology after crevice test

Various types of rust morphologies have been observed on the corroded surfaces of MPS specimens after the crevice test in 3.5 wt.% NaCl solution. Earlier Raman spectroscopy (Fig. 5) shows that the corroded surfaces of all the MPS specimens contain similar types of rust phases such as α FeOOH, γ FeOOH, β FeOOH and α Fe_2O_3.

In addition, SEM microscopy has been used for the rust phase analysis. Fig. 6 shows the various types of rust morphologies formed on the corroded surface of the MPS specimen developed by austempering at 300^0C after 0 s of continuous cooling for the representation purpose. Other MPS specimens also have similar types of rust morphologies. Needle or whisker like morphology indicates the presence of α FeOOH (Fig. 6a), while the flower petal like morphology denotes the presence of γ FeOOH in the corrosion products (Fig. 6b). Previous studies have also reported similar types of whiskers and flower petals like morphologies for α FeOOH and γ FeOOH, respectively, in the rust phases.[36–38] Furthermore, Fig. 6c shows the rod type crystals which reveal the presence of β FeOOH in the rust products. Alcantara et al. have reported the whiskers and flower petals of α FeOOH and γ FeOOH, respectively, in the case of rust formed on the surface of the carbon steel exposed in the marine environment.[29] Furthermore, various researchers have reported the presence of β FeOOH in the rust products of the steel when exposed to the chloride containing environment.[31–33] Alcantara et al. [29] and Fuente et al. have also observed the similar rod type morphology of the β FeOOH in the rust products of steels exposed to the chloride containing environment.[29,39] Fig. 6d shows the morphology of α Fe_2O_3. Sayed et al. and Zhu et al. have also observed a similar spherical morphology of Fe_2O_3.[40,41]

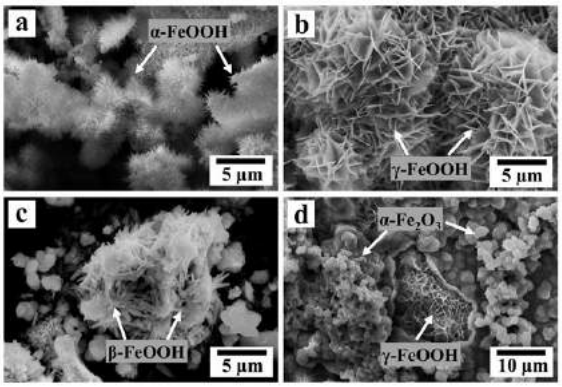


Figure 6. SEM micrographs of the various types of rust formed on the MPS specimen (300^0C- 0 s) after the crevice test in 3.5 wt.% NaCl solution.

The presence of α FeOOH increases the stability of the rust products, and this provides the compact and dense protective rust layer.[38] Therefore, the presence of a high amount of α FeOOH corresponding to the high PAI represents the formation of protective rust layer in the MPS specimens. Though similar rust phases have been formed in the corrosion products of all the MPS specimens, their phase fractions are observed to vary for each MPS specimen. These fractions have been calculated with the help of Raman spectra, as explained above. The variation in the rust phase (α FeOOH, β FeOOH, γ FeOOH and α Fe_2O_3) fractions could be influenced by the microstructural variation and presence of various microstructural constituents such as bainite, IF, RA and pearlite in the MPS specimens.

3.3.4 Surface morphologies of the MPS specimens after the crevice test

Furthermore, the surface morphologies of the MPS specimens after the crevice test in 3.5 wt.% NaCl solution have been analysed using SEM micrographs. Fig. 7 shows the MPS specimen after 9 months of

the crevice test in 3.5 wt.% NaCl solution. Here, MPS specimen developed by austempering at 300^{0}C without a cooling step has been shown for the representation purpose. Morphological studies of the exposed surfaces of the MPS specimens using the SEM micrographs have been performed on two different regions 1 and 2. Here, region 1 is the crevice region and region 2 is the non crevice region. It is worth mentioning that the exposed surfaces of the MPS specimens have been cleaned properly before the surface analysis. The crevice corrosion is located in a small region but propagates orders of magnitude much faster than the general/uniform corrosion. The affected small and localized area results in the formation of pits. In starting stage of crevice corrosion, the oxidation and reduction reactions take place uniformly, even in the crevice region. After some time, depletion of oxygen occurs within the crevice region, which restricts the convection process. In contrast, metal dissolution continues resulting in the excessive positive ions and migration of the chloride ions from NaCl solution within the crevice region. In an aqueous solution, the metal chloride forms metal hydroxide and free HCl acid.

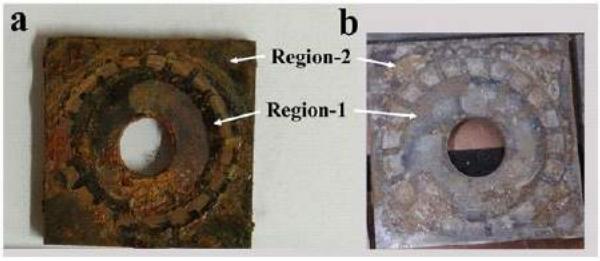


Figure 7. MPS specimen (developed by austempering at 300^{O}C without a cooling step) after 9 months of the crevice test in 3.5 wt.% NaCl solution (a) before cleaning and (b) after cleaning with Clark's solution.

Fig. 8 shows the SEM micrographs of the crevice regions (region 1, as shown in Fig. 7) of the MPS specimens (developed at various combinations of continuous cooling durations and austempering temperatures). Fig. 8a represents the crevice region of the MPS specimen developed by austempering at 300^{O}C after 0 s continuous cooling. Here, the dissolution of the crevice surface looks like a deep etched structure. Shallow pits have also been observed on the crevice surface as shown by arrowheads (Fig. 8a). The dissolution of the crevice surface and the severity of pits have increased with the increase of the continuous cooling durations till 20 s (Fig. 8a c). It could be due to the increase of IF and RA volume fractions and decrease of bainite volume fraction with the increase of continuous cooling duration at a particular austempering temperature (Table I). Furthermore, the dissolution of the MPS specimen decreases with a further increase of continuous cooling beyond 20 s (Fig. 8d). It could be due to the formation of pearlite which surpasses the effect of the increased fraction of IF at 40 s continuous cooling. In addition, RA formation decreases at 40 s continuous cooling which further helps in decreasing the dissolution of MPS specimen at 40 s. Similar trends of dissolution and severity of the pits have been observed for the MPS specimens developed by austempering at 350^{0}C and 400^{0}C after different continuous cooling durations (Fig. 8e h and i l).

It has also been observed from Fig. 8 that the MPS specimens developed at 300^{O}C austempering exhibit lower dissolution as compared to the MPS specimens developed by austempering at 350^{O}C and 400^{O}C after the corresponding continuous cooling durations. It could be due to the formation of a lower bainitic structure at 300^{O}C austempering, resulting in the uniform and lower dissolution of the crevice surface of the MPS specimens (Fig. 8a d). The specimens austempered at 350^{O}C and 400^{O}C, the presence of RA near the grain boundary and within the bainitic structure results in the higher dissolution of the MPS specimens (Fig. 8e h and i l).

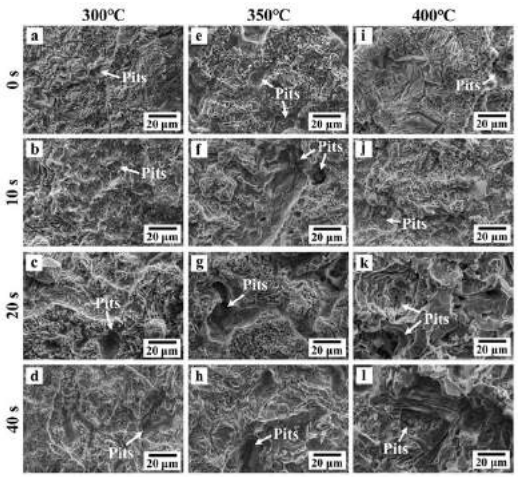


Figure 8. SEM micrographs of the MPS specimens at the crevice region after crevice test in 3.5 wt.% NaCl solution, austempered at 300^{O}C, 350^{O}C and 400^{O}C with various combinations of continuous cooling 0 s, 10 s, 20 s and 40 s.

Fig. 9 shows the SEM micrographs of the non crevice region (region 2, as shown in Fig. 7) of the MPS specimens after 9 months of crevice test in 3.5 wt.% NaCl solution. Variation in the corrosion attack of all the MPS specimens as shown in Fig. 9 could be due to the presence of different bainitic morphologies and variation in the phase/micro constituent fractions of the MPS specimens. Non crevice regions of the MPS specimens after the crevice tests show the characteristic microstructures (etch like) as shown in Fig. 2 after etching with nital. It is worth mentioning that no etching has been performed on the MPS specimens before or after the crevice corrosion test. The etch like morphology formed on the exposed surface of the MPS specimens after the crevice test could be due to the electro polishing effect.

The uniform dissolution has been clearly seen throughout the exposed surface of the MPS specimens. For all three austempering temperatures, the MPS specimens developed without a cooling step show lowest surface dissolution compared to the other MPS specimens with 10 s, 20 s and 40 s of continuous cooling before austempering. It could be due to the presence of lower RA fraction and absence of IF phase in the MPS specimens developed without any continuous cooling step (0 s of continuous cooling) before austempering (Table I). It can be clearly seen from Fig. 9 that the severity of dissolution increases with the increase of continuous cooling duration till 20 s. It could be due to increase of RA fraction and formation of IF with the increase of continuous cooling duration till 20 s. The enhanced galvanic corrosion due to the increase of active phases (RA and IF) attributes to the increase of dissolution of the MPS specimens till 20 s of continuous cooling. It can be seen from Table I that beyond 20 s of continuous cooling, pearlite starts forming beside bainite, RA and IF. It is to be noted that beyond 20 s of continuous cooling, fractions of bainite and RA decrease whereas IF fraction increases and the formation pearlite takes place in the MPS specimens (Table I). Since volume fraction of IF increases, the galvanic couple spreads out between larger area IF and pearlite, where IF is an active phase and pearlite as whole acts as a cathode resulting in the reduced galvanic effect. Pearlite acting as cathode has been clearly shown by Katiyar et al.[2,17] This leads to the reduction of dissolution and severity of pits on the exposed surface of the MPS specimen (austempering at 300^{0}C) developed at 40 s of continuous cooling compared to than that of 20 s. This anomalous behaviour is also confirmed by the marginal decrease in corrosion rate obtained after the crevice tests.

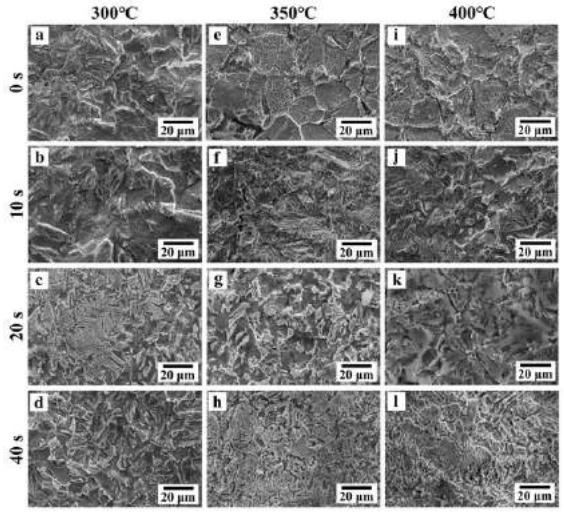


Figure 9. SEM micrographs of the MPS specimens of the non crevice region after crevice test in 3.5 wt.% NaCl solution, austempered at 300^{0}C, 350^{0}C and 400^{O}C with various combinations of continuous cooling 0 s, 10 s, 20 s and 40 s.

Optical profilometry has been further carried out to understand the surface morphologies of the MPS specimens after the crevice test. Fig. 10 shows the optical profilometry images (3D) of the exposed surfaces of the MPS specimens (developed at various combinations of austempering temperatures and continuous cooling durations) after the crevice test in 3.5 wt.% NaCl solution. It is worth mentioning that the MPS specimens have been cleaned properly to remove the rust from the exposed surfaces before the optical profilometry analysis. Pits type morphology on the exposed surfaces of the MPS specimens can be clearly seen from these images (Fig. 10). The average surface roughness (R_a) and pit depths (R_v) are obtained from the optical profilometry and given in Table II.

It is worth mentioning that the severity of the attack on all the MPS specimens has been taken as the measurement of average surface roughness and pit depths. The average surface roughness and pit depth have been found to be lowest for the MPS specimen with 0 s of continuous cooling and austempered at 300ºC. Overall, roughness and pit depths of all the

MPS specimens have been observed to increase with the increase of continuous cooling up to 20 s. There is a drop in the average surface roughness and pit depth with a further increase in the continuous cooling to 40 s. Hence, the severe attack has been noticed for 20 s of continuous cooling of the MPS specimens austempered at all three temperatures. Whereas, it has been observed to be least for 0 s continuous cooling of the MPS specimens austempered at all three temperatures.

The variation in the surface roughness and pit depth of the MPS specimens could be due to the presence of various phases/microconstituents and their fractions. The continuous decrease of bainite volume fraction and increase of IF volume fraction result in the increase of dissolution at the grain boundary up to 20 s of continuous cooling for all three austempering temperatures. This has been confirmed by the surface roughness and pit depths (Table II) of the MPS specimens after the crevice test that R_a and R_v increase up to 20 s of continuous cooling. Beyond 20 s, pearlite starts forming and reduces the dissolution, which further reduces the roughness and pit depths (Table II). Interestingly, the R_a and R_v obtained from the optical profilometry are corroborated well with the result of corrosion rate (Table II) obtained from the gravimetric method (weight loss methods). Hence, the higher average values of roughness and pit depth indicate the higher dissolution of steels resulting in a higher corrosion rate. Interestingly, the PAI values obtained from all the corroded steel specimens have followed the exact opposite trend of R_a, R_v and the corrosion rate (Table II).

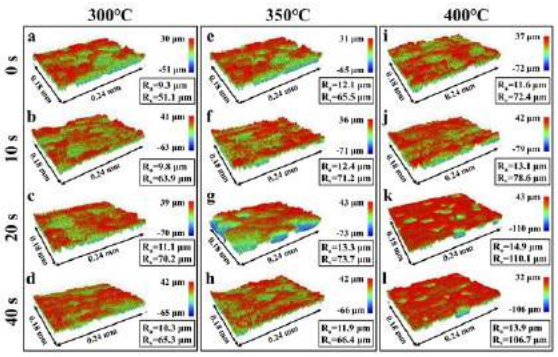


Figure 10. Results obtained from optical profilometry analysis over the entire measure array of the corroded surface of the MPS specimens after the crevice tests in 3.5 wt.% NaCl solution, austempered at 300^{0}C: (a) 0 s, (b) 10 s, (c) 20 s and (d) 40 s continuous cooling time; at 350^{0}C: (e) 0 s, (f) 10 s, (g) 20 s and (h) 40 s continuous cooling time; and at 400^{0}C: (i) 0 s, (j) 10 s, (k) 20 s and (l) 40 s continuous cooling time. (R_a: average surface roughness, R_v: pit depth)

3.3.5 Correlation of the corrosion rate, R_a and PAI obtained from the crevice test with the continuous cooling durations and austempering temperatures of the MPS specimens

Figs. 11a, b and c show the correlation between the corrosion rate, R_a and PAI of the MPS specimens (developed at various austempering temperatures such as 300^{0}C, 350^{0}C and 400^{0}C) after the crevice test in 3.5 wt.% NaCl solution after various continuous cooling durations (0 s, 10 s, 20 s, and 40 s), respectively.

It can be seen from Fig. 11a that at a particular austempering temperature of the MPS specimens, the corrosion rate increases with the increase of continuous cooling durations till 20 s and decreases with a further increase of cooling durations to 40 s. MPS specimens austempered at 300^{0}C shows lower corrosion rates for all four continuous cooling durations than other austempering temperatures (350^{0}C and 400^{0}C) with corresponding continuous cooling durations. It can also be seen from Fig. 11a that at a corresponding continuous cooling duration, the increase in the corrosion rate of the MPS specimens from 350^{0}C to 400^{0}C austempering is higher compared to the increase of corrosion rate from 300^{0}C to 350^{0}C austempering.

Similarly, for a particular austempering temperature, the average surface roughness of the MPS specimens increase with the increase of continuous cooling durations till 20 s and decrease beyond that (Fig. 11b). A similar trend of corrosion rate and surface roughness have been observed for all three austempering temperatures of the MPS specimens. It can be clearly seen that the PAI values are in inverse relation to the corrosion rate and surface roughness of the MPS specimens (Figs. 11a, b and c). The PAI value decreases with the increase of continuous cooling duration of the MPS specimens till 20 s and increases beyond that (Fig. 11c). MPS specimens austempered at 300^{0}C show higher PAI values than the MPS specimens austempered at 350^{0}C and 400^{0}C (Fig. 8c).

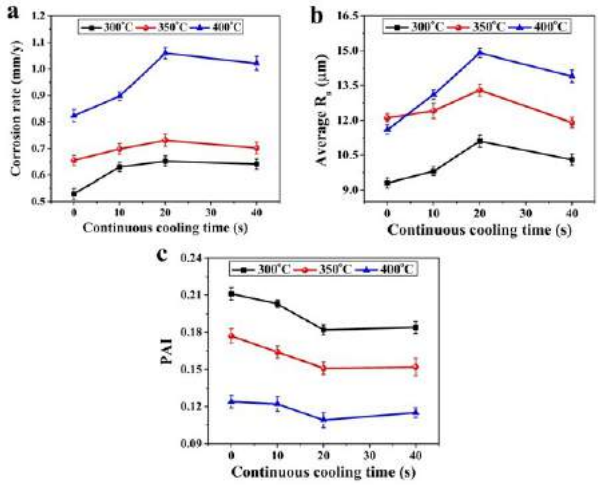


Figure 11. Correlation of (a) corrosion rate, (b) R_a and (c) PAI with the variation of continuous cooling durations of MPS specimens after the crevice tests in 3.5 wt.% NaCl solution.

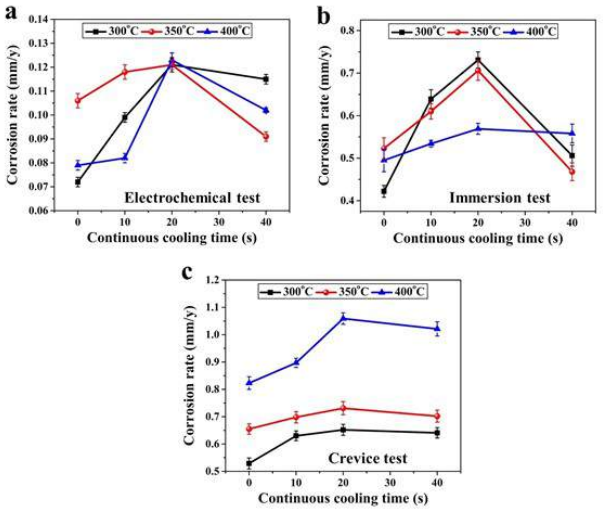


Figure 12. Comparison of variation of CR with austempering temperatures and continuous cooling time of the MPS specimens after (a) electrochemical test,[23] (b) immersion test and (c) crevice test in 3.5 wt.% NaCl solution.

3.3.6 Relation of CR obtained from the electrochemical, immersion and crevice tests with continuous cooling durations and austempering temperatures of the MPS specimens

Figs. 12 a, b and c show the corrosion performance of the MPS specimens obtained from various corrosion techniques such as electrochemical test,[22] immersion test (30 days) and crevice test (9 months), respectively, in 3.5 wt% NaCl solution. It is worth mentioning that the electrochemical and immersion tests of the MPS specimens have been performed by the current authors.[23] It can be clearly seen from all three corrosion tests (electrochemical, immersion and crevice) that the corrosion rate is least for the MPS specimen austempered at a particular temperature without any prior cooling step. However, the MPS specimen developed by austempering at 300^{O}C after 0 s of continuous cooling shows the lowest corrosion rate.

In a nutshell, the corrosion susceptibility of the MPS specimens made at all the austempering temperatures after 20 s of continuous cooling has increased due to the presence of a higher volume fraction of RA as well as of IF phase. Since RA and IF both are present in a higher amount at this condition, the possibility of formation of the number. In a nutshell, the corrosion susceptibility of the MPS specimens made at all the austempering temperatures after 20 s of continuous cooling has increased due to the presence of a higher volume fraction of RA as well as of IF phase. Since RA and IF both are present in a higher amount at this condition, the possibility of formation of the number of galvanic couples are expected to increase. However, in the steel specimens with 40 s continuous cooling, the corrosion susceptibility has decreased as compared to the steel specimens with 20s of continuous cooling due to the low volume fraction of RA and the presence of fine pearlite. Therefore, it can be stated that the presence of the RA in the C enriched state adversely affects the corrosion behaviour of the MPS specimens. The variation of the corrosion rate, R_p, R_{ct}, R_a, R_v and PAI is attributed to the different microstructures and the distribution of various constituent phases present in the MPS specimens and their subsequent formation of micro galvanic couples.

In addition, Table III shows the comparative mechanical and corrosion properties of the multiphase steel (developed by 0 s of continuous cooling followed by austempering at 300^{O}C) with the existing elastic rail clip.[21,23,24,42] Here, the corrosion and wear analysis of the multiphase steel and existing elastic rail clip are performed by the current authors. It is worth mentioning that the electrochemical and

Table III. Comparison of mechanical and corrosion properties of the multiphase steels as determined in the present analysis with the existing elastic rail clip.[21,23,24,42]

		Multiphase steel (300^{O}C 0s)	Existing elastic rail clip
Mechanical properties	YS (MPa)	1450±18	1338±14
	UTS (MPa)	1995±25	1482±18
	% Elongation	10.5±1.5	6.4±0.2
Wear	Wear volume loss (40 N load) (mm^3)	0.175±0.012	0.547±0.018
	Specific wear rate ($mm^3.N^{-1}.m^{-1}x10^{-4}$)	0.232±0.017	0.725±0.034
Corrosion properties	Electrochemical test (mm/y)	0.072±0.002	0.105±0.017
	Crevice test (mm/y)	0.529±0.020	0.958±0.031

crevice test of both the steels (multiphase and existing elastic rail clip) were performed in 3.5 wt.% NaCl solution. For the scientific comparative tests, the concentration of 3.5% of NaCl (by weight) in aqueous solution is often used as the salinity level in seawater is relatively constant, at about 35 ppt (35,000 mg/L or 35,000 ppm or 3.5% NaCl). Also, ASTM standard recognises 0.6 molar NaCl solution in its standard which is equivalent to 3.5%. The test electrolyte in most academic corrosion studies has been considered as 3.5 wt.% NaCl as per the ASTM Standard-G44.[43] Hence, we have considered 3.5 wt.% NaCl solution in the present work for the crevice corrosion studies. It can be clearly seen from Table III that the corrosion rates of the multiphase steel obtain from both the electrochemical and crevice test are much lower than that of the existing elastic rail clip steel. Multiphase steel also shows superior mechanical properties than that of the existing elastic rail clip steel. So, the multiphase steel showing better mechanical, corrosion and wear properties could be an alternative to the existing elastic rail clip steel.

4. Conclusions

- Multiphase steel (MPS) specimens developed from the EN 45 grade steel using austempering at 300^{O}C, 350^{O}C and 400^{O}C after continuous cooling of 0 s, 10 s, 20 s and 40 s consist of various fractions of bainite, RA, intercritical ferrite (IF) and pearlite.
- Bainitic morphology has changed from lower to mixed and upper bainite with the austempering from 300^{O}C to 350^{O}C and 400^{O}C, respectively. For all the austempering temperature, bainite fraction decreases and IF fraction increases continuously with the increase of continuous cooling time. RA fraction increases till 20 s of continuous cooling and decreases beyond that. Pearlite forms in the MPS specimens only when continuous cooling exceeds 20 s.
- The corrosion rates of the MPS specimens obtained from the crevice tests for all three austempering temperatures gradually increase with the increase in continuous cooling till 20 s followed by a decrease in corrosion rate with 40 s of continuous cooling.

- SEM micrographs reveal that the dissolution of the crevice surface looks like a deeply etched structure with some distributed shallow pits. The dissolution of the crevice surface and the severity of pits have been observed to be lower for the MPS specimens austempered at 300^{O}C as compared to the 350^{O}C and 400^{O}C austempering.

- SEM and Raman spectroscopy reveal the presence of various rust phases on exposed surfaces of the MPS specimens after the crevice test. Similar rust phases with varying fractions could be due to the presence of different phases/ microconstituents (such as bainite, IF, RA and pearlite) and their different volume fractions in the MPS specimens.

- The PAI values of the MPS specimens austempered at all three temperatures without continuous cooling are found to be highest as compared to the other cooling durations of the respective austempering temperature. The average surface roughness (R_a) obtained from the optical profilometry is corroborated well with the corresponding PAI values and corrosion rates.

References

[1] H.A. Aglan, Z.Y. Liu, M.F. Hassan, and M. Fateh, "Mechanical and fracture behavior of bainitic rail steel," *J. Mater. Process. Technol.*, **151**, 268 (2004).

[2] P. K. Katiyar, S. Misra, and K. Mondal, "Comparative Corrosion Behavior of Five Microstructures (Pearlite, Bainite, Spheroidized, Martensite, and Tempered Martensite) Made from a High Carbon Steel," *Metall. Mater. Trans. A Phys. Metall. Mater. Sci.*, **50**, 1489 (2019).

[3] X. Y. Long, F. C. Zhang, J. Kang, B. Lv, and X. B. Shi, "Materials Science & Engineering A Low temperature bainite in low carbon steel," *Mater. Sci. Eng. A*, **594**, 344 (20141).

[4] R. Bakhtiari, and A. Ekrami, "The effect of bainite morphology on the mechanical properties of a high bainite dual phase (HBDP) steel," *Mater. Sci. Eng. A*, **525**, 159 (2009).

[5] K. Abbaszadeh, H. Saghafian, and S. Kheirandish, "Effect of Bainite Morphology on Mechanical Properties of the Mixed Bainite martensite Microstructure in D6AC Steel," *J. Mater. Sci. Technol.*, **28**, 336 (2012).

[6] C. Zhang, B. Liao, D. Cai, T. Zhao, and Y. Fan, "Development of hot rolled dual phase weathering steel Cu P Cr Ni Mo," *Mater. Des.*, **28**, 1760 (2007).

[7] J.I. Barraza fierro, B. Campillo illanes, and X. Li, "Steel Microstructure Effect on Mechanical Properties and Corrosion Behavior of High Strength Low Carbon Steel," **45A**, 3981 (2014).

[8] Z. Changle, L. Shouhai, F. Hanguang, and L. Yinghua, "Microstructure evolution and wear resistance of high silicon bainitic steel after austempering," *Integr. Med. Res.*, **9**, 4826 (2020).

[9] H. Amel farzad, H.R. Faridi, F. Rajabpour, A. Abolhasani, S. Kazemi, and Y. Khaledzadeh, "Materials Science & Engineering A Developing very hard nanostructured bainitic steel," *Mater. Sci. Eng. A*, **559**, 68 (2013).

[10] H.K.D.H. Bhadeshia, *Bainite in steels: Transformation, Microstructure and Properties,* IOM Communications Ltd., London, UK, Second edition, 2001.

[11] H.K.D.H. Bhadeshia, "High Performance Bainitic Steels," *Mater. Sci. Forum*, **500–501**, 63 (2005).

[12] A. P. Moon, "Corrosion Behavior of Pearlitic / Ferritic Pearlitic and Bainitic Rail, Axle and Wheel steels," PhD Thesis, Indian Institute of Technology Kanpur, India, 2014.

[13] J. Guo, S. Yang, C. Shang, Y. Wang, and X. He, "Influence of carbon content and microstructure on corrosion behaviour of low

alloy steels in a Cl containing environment," *Corros. Sci.*, **51**, 242 (2009).

[14] W. Handoko, and F. Pahlevani, "Enhancing Corrosion Resistance and Hardness Properties of Carbon Steel through Modification of Microstructure," *Mater*, **11**, 2404 (2018).

[15] D. Zhang, X. Gao, G. Su, Z. Liu, N. Yang, L. Du, and R.D.K. Misra, "Effect of Tempered Martensite and Ferrite / Bainite on Corrosion Behavior of Low Alloy Steel Used for Flexible Pipe Exposed to High Temperature Brine Environment," J. *Mater. Eng. Perform*, **27**, 4911 (2018).

[16] S. Qu, X. Pang, Y. Wang, and K. Gao, "Corrosion behavior of each phase in low carbon microalloyed ferrite bainite dual phase steel: Experiments and modeling," *Corros. Sci.*, **75**, 67 (2013).

[17] P.K. Katiyar, S. Misra, and K. Mondal, "Effect of Different Cooling Rates on the Corrosion Behavior of High Carbon Pearlitic Steel," *J. Mater. Eng. Perform.*, **27**, 1753 (2018).

[18] O. Kazum, M. Bobby Kannan, H. Beladi, I. B. Timokhina, P. D. Hodgson, and S. Khoddam, "Aqueous corrosion performance of nanostructured bainitic steel," *Mater. Des.*, **54**, 67 (2014).

[19] Z.F. Wang, L.X. Wu, Y.Q. Sun, and R. D. Han, "The effect of the microstructure on the corrosion resistance of bainitic steel," *Phys. Examination Test*, **4**, 37 (2011).

[20] K. Singh, and A. Singh, "Comparative electrochemical impedance spectroscopy study in chloride environment of nano structured bainitic steels prepared by austempering at varied temperatures" *Eng. Research Express*, **2**, 035040 (2020).

[21] A. Varshney, S. Sangal, S. Kundu, and K. Mondal, "Super strong and highly ductile low alloy multiphase steels consisting of bainite, ferrite and retained austenite," *Mater. Des.*, **95**, 75 (2016).

[22] A. Varshney, S. Sangal, A. K. Pramanick, and K. Mondal, "Microstructural evidence of nano carbides in medium carbon high silicon multiphase steels," *Mater. Sci. Eng. A*, **708**, 237 (2017).

[23] Neetu, P.K. Katiyar, S. Sangal, K. Mondal, Effect of various phase fraction of bainite, intercritical ferrite, retained austenite and pearlite on the corrosion behavior of multiphase steels, *Corros. Sci.*, **178**, 109043 (2021).

[24] Neetu, S. Sangal, K. Mondal, Effect of various phase fraction of bainite, intercritical ferrite, retained austenite and pearlite on the wear behavior of multiphase steels, *Wear*, **500–501**, 204355 (2022).

[25] H. Bhadeshia, "Materials Algorithm Project Program Library," Phase Transformation Group, Department of Materials Science and Metallurgy, University of Cambridge, Cambridge, United Kingdom, https://www.phase trans.msm.cam.ac.uk/map/steel/programs/mucg46 b.html.

[26] ASTM Standard G78 15, "Standard Guide for Crevice Corrosion Testing of Iron Base and Nickel Base Stainless Alloys in Seawater and Other Chloride Containing Aqueous Environments," ASTM International, West Conshohocken, PA, 2015.

[27] J. Aramendia, L. Gomez Nubla, L. Bellot Gurlet, K. Castro, C. Paris, P. Colomban, and J.M. Madariaga, "Protective ability index measurement through Raman quantification imaging to diagnose the conservation state of weathering steel structures," *J. Raman Spectrosc.*, **45**, 1076 (2014).

[28] ASTM G1 03, "Standard Practice for Preparing, Cleaning, and Evaluating Corrosion Test Specimens," ASTM International, West Conshohocken, PA, 2017.

[29] J. Alcántara, B. Chico, J. Simancas, I. Díaz, D.D.L. Fuente and M. Morcillo, "An attempt to classify the morphologies presented by

different rust phases formed during the exposure of carbon steel to marine atmospheres," *Mater. Charact.*, **118**, 65 (2016).

[30] P.K. Katiyar, P.K. Behera, and S. Misra, "Effect of Microstructures on the Corrosion Behavior of Reinforcing Bars (Rebar) Embedded in Concrete," *Met. Metar. Int.*, **25**, 1209 (2019).

[31] B. Panda, R. Balasubramaniam, and G. Dwivedi, "On the corrosion behaviour of novel high carbon rail steels in simulated cyclic wet dry salt fog conditions," *Corros. Sci.*, **50**, 1684 (2008).

[32] A. Demoulin, C. Trigance, D. Neff, E. Foy, P. Dillmann, and V. L. Hostis, "The evolution of the corrosion of iron in hydraulic binders analysed from 46 and 260 year old buildings," *Corros. Sci.*, **52**, 3168 (2010).

[33] S. Réguer, P. Dillmann, and F. Mirambet, "Buried iron archaeological artefacts: Corrosion mechanisms related to the presence of Cl containing phases," *Corros. Sci.*, **49**, 2726 (2007).

[34] P.K. Katiyar, P.K. Behera, S. Misra, and K. Mondal, "Comparative Corrosion Behavior of Five Different Microstructures of Rebar Steels in Simulated Concrete Pore Solution with and Without Chloride Addition," *J. Mater. Eng. Perform.*, **28**, 6275 (2019).

[35] S. Choudhary, A. Garg, and K. Mondal, "Relation Between Open Circuit Potential and Polarization Resistance with Rust and Corrosion Monitoring of Mild Steel," *J. Mater. Eng. Perform.*, **25**, 2969 (2016).

[36] J. Yang, Y. Lu, Z. Guo, J. Gu, and C. Gu, "Corrosion behaviour of a quenched and partitioned medium carbon steel in 3.5 wt.% NaCl solution," *Corros. Sci.*, **130**, 64 (2018).

[37] R. Sun, Q. Yu, Y. Zhang, X. Yan, Y. Lu, C. Zhang, and Q. Wang, "Effect of Si Content on the Corrosion Behavior of 420 MPa Weathering Steel," *Metals*, **9**, 486 (2019).

[38] P. Dhaiveegan, N. Elangovan, T. Nishimura, and N. Rajendran, "Weathering Steel in Industrial Marine Urban Environment: Field Study," *Mater. Trans.*, **57**, 148 (2016).

[39] D.D.L. Fuente, J. Alcántara, B. Chico, I. Díaz, J. A. Jiménez, and M. Morcillo, "Characterisation of rust surfaces formed on mild steel exposed to marine atmospheres using XRD and SEM/Micro Raman techniques," *Corros. Sci.*, **110**, 253 (2016).

[40] F.N. Sayed, and V. Polshettiwar, "Facile and Sustainable Synthesis of Shaped Iron Oxide Nanoparticles: Effect of Iron Precursor Salts on the Shapes of Iron Oxides," *Sci. Rep.*, **5**, 9733 (2015).

[41] J. Zhu, L. Li, Z. Xiong, Y. Hu, and J. Jiang, "Evolution of Useless Iron Rust into Uniform α Fe_2O_3 Nanospheres: A Smart Way to Make Sustainable Anodes for Hybrid Ni-Fe Cell Devices," *ACS Sustainable Chem. Eng.*, **5**, 269 (2017).

[42] Neetu, "Corrosion and wear behaviour of the multiphase bainitic Elastic Rail Clip and EN 45 grade steels," PhD Thesis, Indian Institute of Technology Kanpur, India, 2022.

[43] ASTM G44-99, Standard Practice for Exposure of Metals and Alloys by Alternate Immersion in Neutral 3.5 % Sodium Chloride Solution, ASTM International, West Conshohocken, PA, 2000.